

MIT Open Access Articles

Aerosol elastic scatter signatures in the near- and mid-wave IR spectral regions

The MIT Faculty has made this article openly available. **Please share** how this access benefits you. Your story matters.

Citation: Richardson, Jonathan M. et al. "Aerosol elastic scatter signatures in the near- and mid-wave IR spectral regions." Laser Radar Technology and Applications XIV. Ed. Monte D. Turner & Gary W. Kamerman. Orlando, FL, USA: SPIE, 2009. 73230Q-9. © 2009 SPIE--The International Society for Optical Engineering

As Published: <http://dx.doi.org/10.1117/12.819165>

Publisher: The International Society for Optical Engineering

Persistent URL: <http://hdl.handle.net/1721.1/52679>

Version: Final published version: final published article, as it appeared in a journal, conference proceedings, or other formally published context

Terms of Use: Article is made available in accordance with the publisher's policy and may be subject to US copyright law. Please refer to the publisher's site for terms of use.



Aerosol Elastic Scatter Signatures in the Near and Mid-Wave IR Spectral Regions

Jonathan M. Richardson¹, John C. Aldridge, Adam B. Milstein, and Joseph J. Lacirignola

¹ MIT Lincoln Laboratory, 244 Wood St., Lexington, MA 02420
richardson@ll.mit.edu

ABSTRACT

An essential milestone in the development of lidar for biological aerosol detection is accurate characterization of agent, simulant, and interferent scattering signatures. MIT Lincoln Laboratory has developed the Standoff Aerosol Active Signature Testbed (SAAST) to further this task, with particular emphasis on the near- and mid-wave infrared.

Spectrally versatile and polarimetrically comprehensive, the SAAST can measure an aerosol sample's full Mueller Matrix across multiple elastic scattering angles for comparison to model predictions. A single tunable source covers the 1.35–5 μm spectral range, and waveband-specific optics and photoreceivers can generate and analyze all six classic polarization states. The SAAST is highly automated for efficient and consistent measurements, and can accommodate a wide angular scatter range, including oblique angles for sample characterization and very near backscatter for lidar performance evaluation.

This paper presents design details and selected results from recent measurements.

Disclaimer: This work was sponsored by the US Army Edgewood Chemical Biological Center under Air Force Contract FA8721-05-C-0002. Opinions, interpretations, conclusions and recommendations are those of the authors and not necessarily endorsed by the United States Government.

1. INTRODUCTION

1.1. Background

Remote ("standoff") detection of biological agents using light detection and ranging (lidar) offers many potential capabilities not provided by point (localized) detection systems. Although point sensors are a more mature technology offering higher localized sensitivity,¹ standoff systems promise sensitivity over a wide area and may be simpler to deploy where this capability is needed. A primary challenge to the development of a reliable bio-Lidar detection system, in that the backscatter coefficient of a potentially dangerous aerosol threat could be small when compared to that of ambient aerosols. It is thus advantageous to be able to detect a threat near its release point where the density is highest, providing early warning to those downwind. Post attack, the standoff system provides information about what locations have been affected, aiding in treatment and decontamination efforts. Ultimately, the best solution for protecting at-risk locations might be an integrated system that combines high-sensitivity point sensors with a wide-area coverage standoff detector, thus providing the best of both worlds.²

Development of standoff detections systems faces a major hurdle in the field test stage due to understandable restrictions on the open release of bio materials. The performance of a particular system must be inferred from a combination of laboratory measurements of threat signatures (using appropriate safety measures), field measurements using benign agent ("simulant") signatures, field measurements of natural and man-made backgrounds, and sensor models. The accuracy of this approach can be verified by measuring signatures of various simulants both in the lab and in the field.

There are various signatures that have been exploited by lidar-based standoff biodetection systems. Some existing bio-lidar concepts have utilized IR backscatter for ranging and sizing combined with UV fluorescence for bio discrimination.³ The fluorescence signature has the complication that it is relatively small (when compared to backscatter) and it lies within the solar band.⁴ It would thus be advantageous to develop methods that rely on infrared signatures only. Recent work has demonstrated that polarization-sensitive infrared lidar may be useful for standoff bio discrimination.⁵⁻⁸ Polarization lidar is sensitive to the size and shape of the aerosols and has been exploited for differentiating ice crystals from water droplets in clouds.⁹ One feature of bio species is that their shape, at least in their

natural form, is highly regular. Even in aggregate form, the underlying shape of individual species is retained. The question is whether this signature is sufficiently selective is best determined by laboratory measurements. Once signatures are measured in the laboratory, detector systems can be developed that exploit them to their best advantage in the field.

Although direct measurements of particle scatter signatures are always preferable, it is very useful to develop aerosol optical models that can predict the scatter. The utility of such models can be illustrated by considering the wide range of conceivable transmitter wavelengths, the many threat and interferent species, the many forms they may take (e.g., agglomerated particles), the infinite possible aerosol mixtures, and the wide range of environmental conditions in which they may be dispersed. Validated aerosol scattering models can help to determine which of these conditions cause significant changes to the agent signatures. Inputs to an aerosol scattering model are the range of particulate/droplet shapes and the real and imaginary indices of refraction. Spherical particles or droplets have optical properties that can be calculated using the Mie method (described in numerous texts). Randomly oriented distributed-sized spheroidal particles (somewhat akin to bacteria) can be calculated straightforwardly using the Mishchenko T-Matrix code.¹⁰ Irregular particles, such as agglomerates, can only be modeled by discrete methods such as the Discrete Dipole Approximation (DDA),¹¹ which involves significant computation, particularly when averaging over many possible sizes and orientations.

MIT Lincoln Laboratory has developed the Standoff Aerosol Active Signature Testbed (SAAST) to measure the polarization-dependent elastic scattering signatures of a variety of biological and inert aerosols over a wide range of wavelengths.¹² The SAAST is both an aerosol ellipsometer and a “lidar in a box.” The SAAST aerosol generation and monitoring system is currently capable of producing a wide range of wet and dry simulant and background aerosols. While the SAAST is currently approved for BL2 (non-pathogenic) biological materials only, many of the measurement techniques would be applicable to laboratory measurements of actual threat agents (to be performed at the appropriate institution using appropriate precautions). The SAAST is able to measure optical scattering near 180° (direct backscatter as in a Lidar system) and also oblique angles. Although most lidar systems are only able to measure at 180°, the oblique scattering data has proven invaluable for comparison to model predictions, as discussed above.

2. DESIGN OF THE SAAST

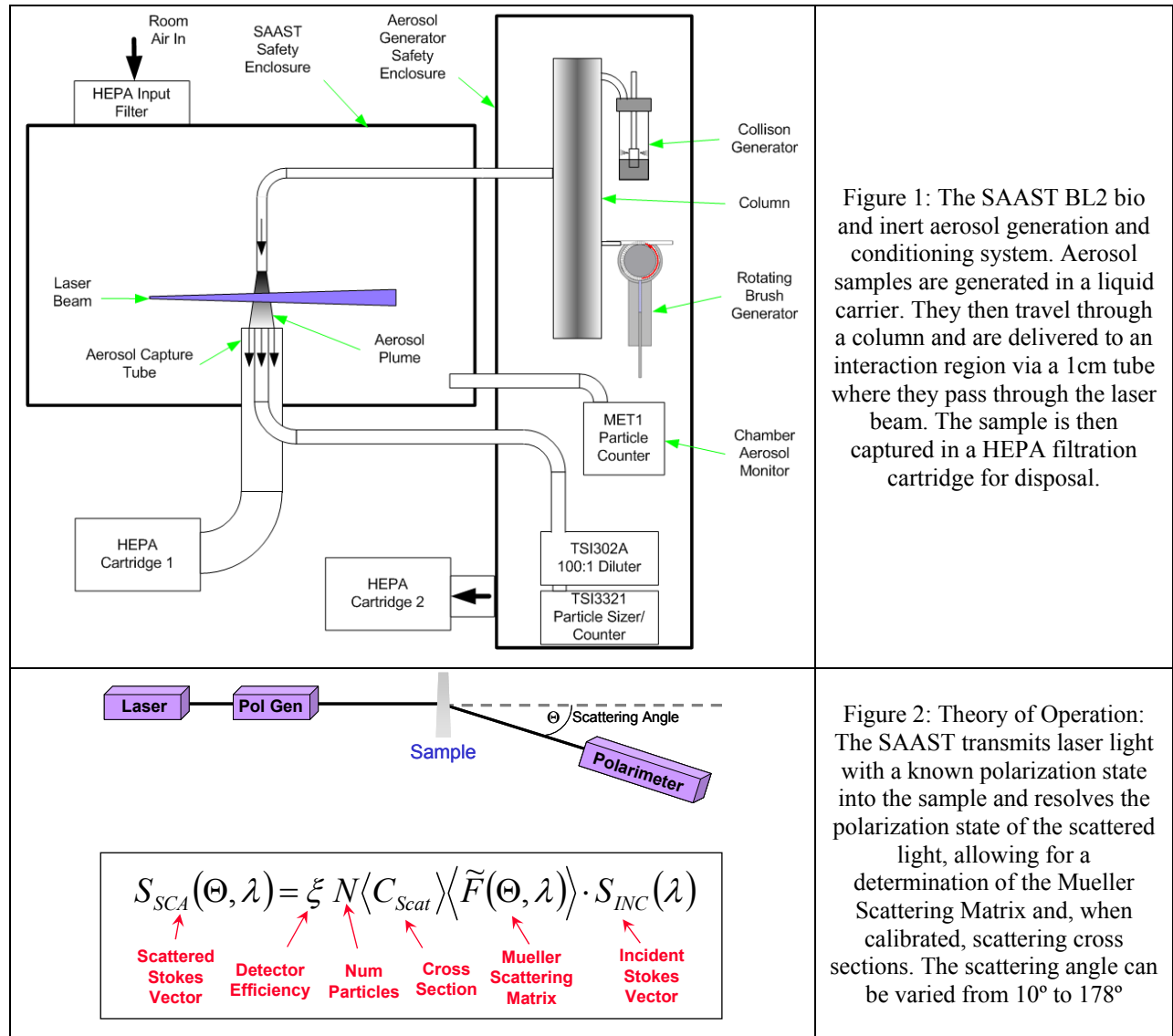
The design of the SAAST is shown in Figure 1. The SAAST is qualified to handle BL1/BL2 (non-pathogenic) bio-aerosols and inert materials. We have used several different aerosolizer systems, both wet and dry. Not shown is the optical receiver system, which rotates in the plane of the laser beam and can measure within 2° of direct backscatter and within 10° of forward at arbitrary increments in between. The optical design has been discussed more thoroughly elsewhere.^{12, 13} The theory of operation is shown in Figure 2. When calibrated and when combined with a particle

counter, the SAAST determines the differential scattering cross section $\left. \frac{d\sigma}{d\Omega} \right|_{\theta}$, which can be integrated to determine

the total scattering cross section σ_{scat} , and the polarization dependence of the scatter. For lidar modeling, the only

quantities of interest are the differential backscatter cross section $\sigma_b \equiv \left. \frac{d\sigma}{d\Omega} \right|_{180^\circ}$, the extinction cross section σ_e , and

the depolarization Δ , defined below. In the case of non-absorbing particles, $\sigma_e = \sigma_{scat}$, and the extinction can be determined by integrating the total scatter. It is always the case that the total scattering cross section places a lower bound on the extinction cross section, the rest being due to absorption.



For aerosols of axial symmetric randomly oriented particles, the Mueller matrix takes on a simplified form as shown below.

$$M(\Theta, \lambda) = \begin{bmatrix} M_{11} & M_{12} & 0 & 0 \\ M_{12} & M_{22} & 0 & 0 \\ 0 & 0 & M_{33} & M_{34} \\ 0 & 0 & -M_{34} & M_{44} \end{bmatrix} \quad (1)$$

M_{11} is known as the scatter function since it describes the relative fraction scattered at each angle.

At back angles, the form is even simpler¹⁴

$$M(180^\circ, \lambda) = M_{11} \begin{bmatrix} 1 & 0 & 0 & 0 \\ 0 & 1 - \Delta & 0 & 0 \\ 0 & 0 & \Delta - 1 & 0 \\ 0 & 0 & 0 & 2\Delta - 1 \end{bmatrix} \quad (2)$$

Where $\Delta = 1 - M_{22}/M_{11}$ is called the depolarization factor¹⁵.

For collections of spheres (e.g., droplets), the Mueller scattering matrix is simplified again

$$M_{sph}(\Theta, \lambda) = \begin{bmatrix} M_{11} & M_{12} & 0 & 0 \\ M_{12} & M_{11} & 0 & 0 \\ 0 & 0 & M_{33} & M_{34} \\ 0 & 0 & -M_{34} & M_{33} \end{bmatrix} \quad (3)$$

Perfect spheres, unlike all non-spherical particles with sizes comparable or larger than the wavelength, cause no depolarization at back angles¹⁵ (e.g., $\Delta = 0$), so $M_{sph}(180^\circ, \lambda) = M_{11}I_{4 \times 4}$, where I is the identity matrix. This has led to the use of Δ as a bio signature, since bacteria and spores are inherently non-spherical.⁷

3. RESULTS

The SAAST is currently involved in an extensive campaign to measure simulant and interferent scattering signatures at 1.55 and 3.4 microns. These signatures are expressed as angle-dependent Mueller scattering matrices, which can be represented as a collection of 6 unique plots, each showing an element of the Mueller matrix vs. scattering angle.¹³ It is common to normalize the unique elements by the scatter function (M_{11}), except for M_{11} itself. There are this six resulting plots that give all the necessary scattering information as shown below.

Our first example is SAAST scattering data taken with an aerosolized collection of 3 micron polystyrene spheres (Duke Scientific) as shown in Figure 3. The data is shown with a comparison to a Mie theory calculation performed for a Gaussian distribution with mean diameter 2.97 microns, standard deviation of .7%, and refractive index of 1.57. The sample is specified to have a mean diameter of 3 microns with <5% standard deviation. Particulars of the fitting procedure are shown in Figure 4. All the elements shown are included in the Chi squared calculation except M_{11} . M_{11} (the scatter function) is not included because this element is highly sensitive to systematic effects (such as aerosol density shifts) during the measurement. The fit to theory is highly sensitive to the mean diameter and real index, providing a viable method for determining both with high accuracy. We also find that the width in the size distribution is much less than the 5% outside tolerance specified.

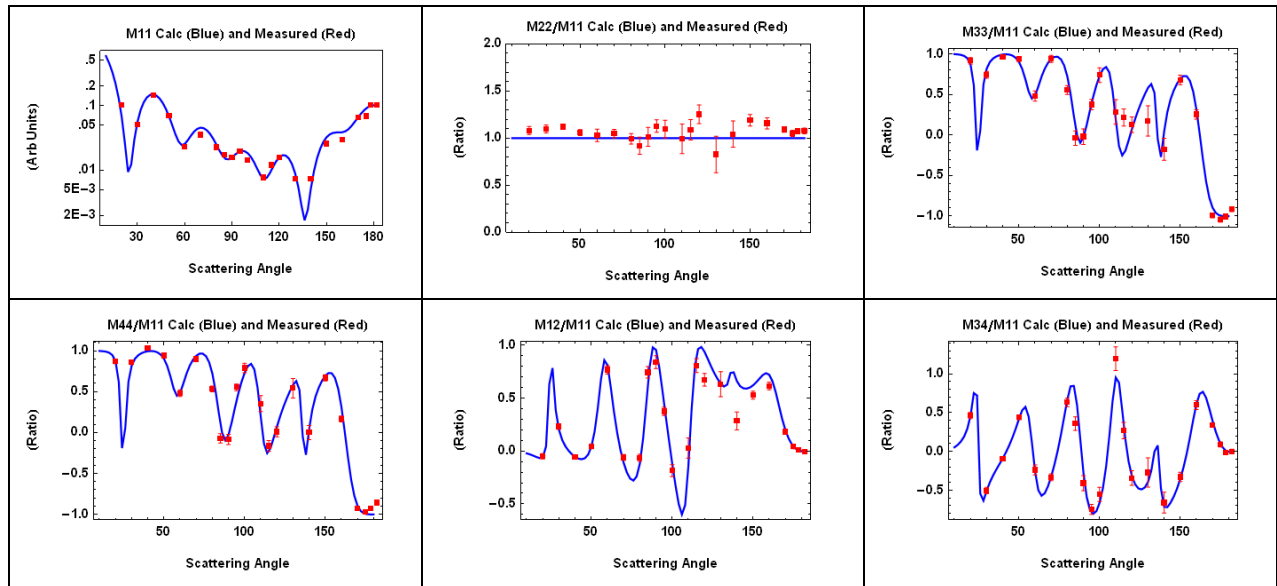
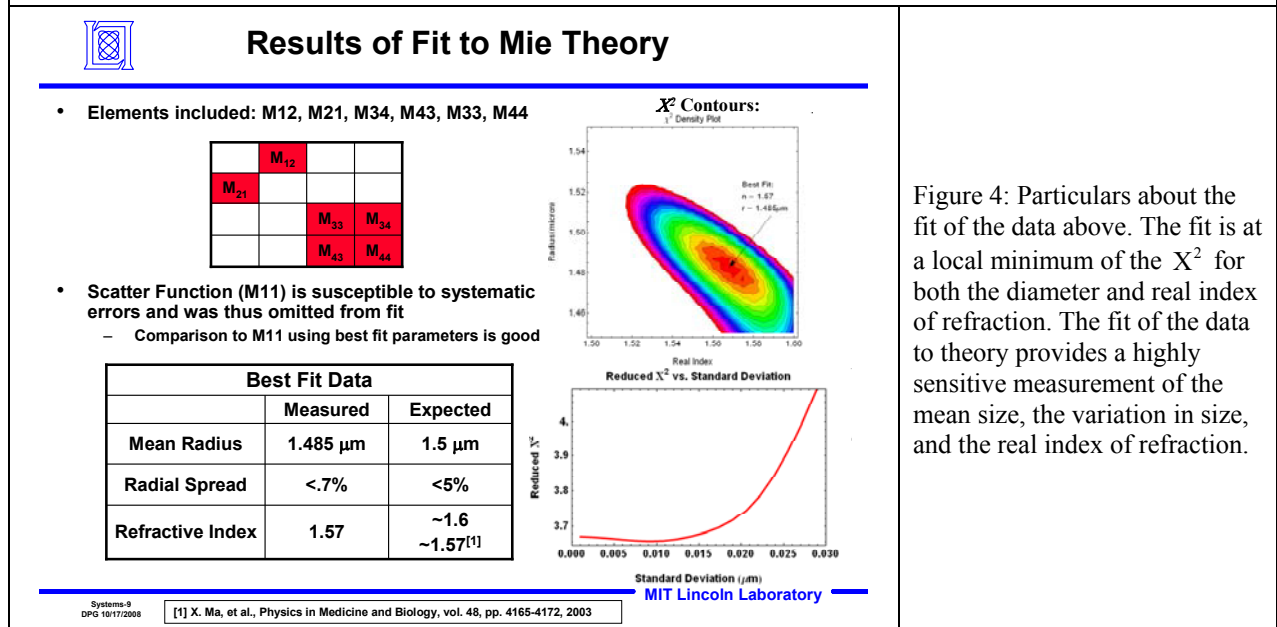


Figure 3: Measured Mueller matrix elements of 3 micron diameter polystyrene spheres at a laser wavelength of 1.55 microns shown with a fit to a Mie-theory calculation as described in the text. M_{11} is also known as the scatter function and has been used to normalize the 5 other elements.



We have previously presented SAAST measurements of bacterial spores¹³. These measurements were uncalibrated and allowed only for the determination of the Mueller scattering matrix. The data shown in Figure 5 was recently acquired using the SAAST at a wavelength of 1.55 μm using liquid-grown *Bacillus atrophaeus* (Bg). We have recently completed a calibration of the SAAST instrument using a calibrated backscatter target from Spherooptics, Inc. It is then possible to get the single-particle differential cross section using the particle count provided by the commercial TSI aerodynamic particle counter depicted in Figure 1. The differential cross section can then be integrated to find the total

scattering cross section as shown in Figure 6. This is a polar integral, meaning that it will be weighted by $\sin(\theta)$, which goes to zero at 0° and 180° . The procedure we have used is to fit a smooth function to the $\sin(\theta)$ -weighted data, including the added zero values, allowing for a straightforward integration of the result to give the total scattering cross section. There are several sources of systematic error in these calculations which are still under study at this time, one of which is the overlap between the laser beam and aerosol plume. We also should have acquired additional data points at the peak of the $\sin(\theta)$ -weighted curve. These uncertainties could lead to a systematic error of at least $\pm 50\%$ on the cross sections, which will be studied in future work.

As in previous work, this data has been compared to an ellipsoidal model, which has been calculated using the Mishchenko T-matrix code, showing that the scatter depends sensitively on the size and shape of the aerosol particles. (Please pardon the use of F rather than M for the elements of the Mueller scattering matrix.) Once again, we find the model parameters that minimize the Chi-squared fitting criterion using all data shown except that of F_{11} , since this element is thought to be more susceptible to systematic error. As shown in the figure, F_{11} (the scatter function) has been normalized to give the differential cross section. At 180° , this is the backscatter cross section in units of μm^2 per steradian. The other elements have all been normalized by F_{11} and are thus unitless. The fitting process is limited by the capability of the Mishchenko code to converge for particles with aspect ratios above $\sim 2.5:1$. We are currently addressing this deficiency using the discrete modeling method outlined below. The model also predicts the cross sections, which can be compared with the measurements. The comparison of the backscatter cross section is very good, whereas the model prediction of the total scatter cross section is approximately twice that measured.

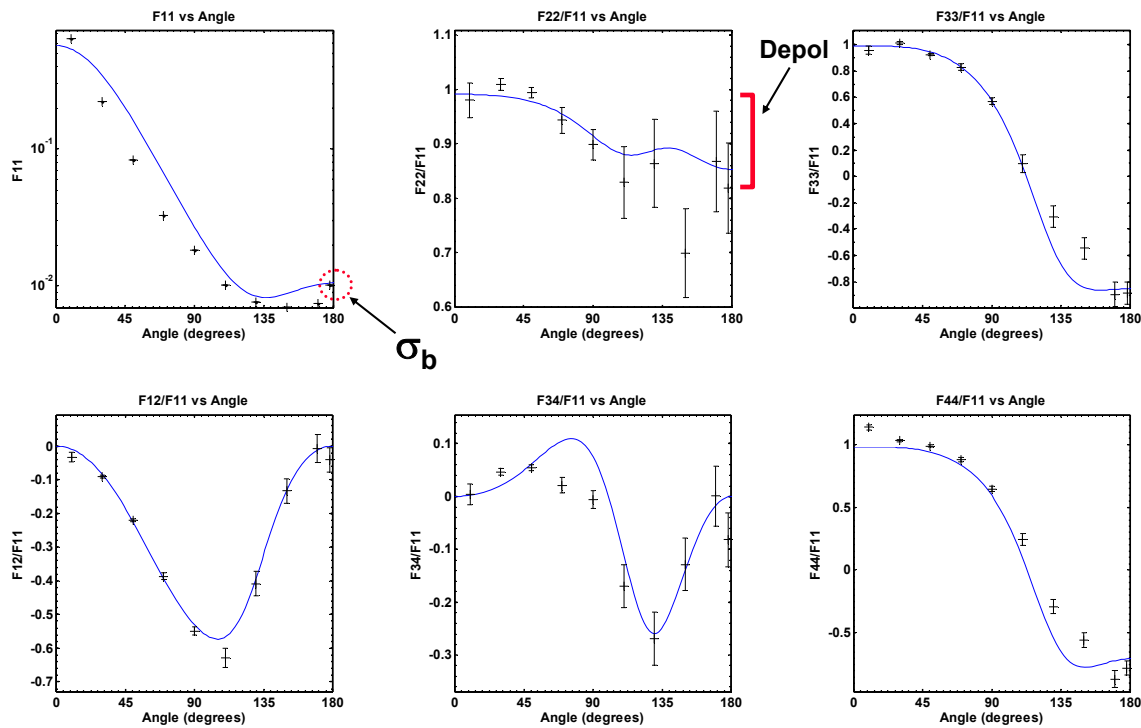
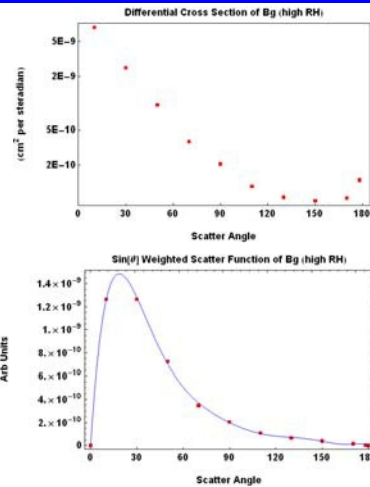


Figure 5: Scatter data from *Bacillus atrophaeus* (Bg) with fit to a T-matrix ellipsoidal model calculated using the Mishchenko code. Model parameters are: Geometric mean diameter: $0.91 \mu\text{m}$, Geometric Stdev: 1.1 (unitless), and Aspect ratio: 0.42. (Please pardon the use of F rather than M for the elements of the Mueller scattering matrix.)



Bg Spore Cross Sections

- **Backscatter cross section**
 $\sigma_b = 1.0 \times 10^{-10} \text{ cm}^2/\text{str}$
- **Depolarization: $14 \pm 7\%$**
- **Weight scatter function data by $\sin^2\theta$ and integrate to obtain the total scattering cross section**
 $\sigma_{\text{scat}} = 7.5 \times 10^{-9} \text{ cm}^2$
- **Model prediction**
 - $\sigma_b = 1.1 \times 10^{-10} \text{ cm}^2/\text{str}$
 - $\sigma_{\text{scat}} = 11 \times 10^{-9} \text{ cm}^2$
 - Depol: 14.7%



BC-18
AM 2/25/2009

MIT Lincoln Laboratory

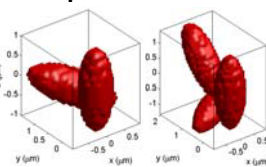
Figure 6: The SAAST can be calibrated such that it is possible to determine the backscatter and total cross sections. The cross sections predicted by the ellipsoidal model compare well with the measured values.

The single spore data shown above is a very special case for a bio aerosol, which can easily agglomerate into particles with several spores. Many such samples have been investigated as part of our measurements program and one example is shown in Figure 8. We are currently developing a system for modeling the scatter from multi-spore clusters as illustrated in Figure 7. Due to the substantial amount of computation that is required, a key enabling technology of this method is LLGRID¹⁶, the high performance, on-demand parallel computing system developed recently at MIT Lincoln Laboratory. We start by obtaining scanning electron microscope (SEM) images of the particulates, which can be used to infer certain spore geometric properties (for example, the aspect ratio). We then model an ensemble of spore clusters by generating numerous instances of discretized volumes consisting of joined spheroid shapes, with the spheroids oriented randomly relative to each other and drawn from a range of sizes. The entire ensemble of modeled spore clusters is then divided among several parallel computing nodes. The Mueller scattering matrix from each individual spore cluster is computed using the Amsterdam DDA code¹⁷. The results from all spore clusters are then aggregated together and averaged using a size distribution which can be adjusted after the fact for optimizing the fit to measured data.

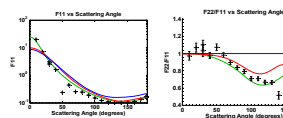
Dry Bg spores clusters



Computational Models



Results



LLGRID



Figure 7: Illustration of the process used to develop a model for multi-spore clusters.

Figure 8 shows some initial example results, including the measured SAST Mueller scattering matrix data for a dry Bg spore sample, and the best fits over size distribution to three different scattering models. The models include Mie theory (i.e., spheres), T-matrix theory (i.e., singleton spheroids) and the DDA (in this case, 3-spheroid clusters). For the T-matrix and the DDA, an aspect ratio of 2.17 to 1 was assumed for consistency with the SEM imagery. To obtain the best fit, a lognormal distribution for each spore's shape was assumed, and the mean and standard deviation which provided the best Chi-squared fit to the measured data were computed. The use of the DDA 3-spheroid model resulted in significant improvements in fitting to the measured data over the other two methods. In particular, note the improved fit to M_{22}/M_{11} (representing shape- and size-dependent depolarization) and to M_{11} (representing the size-dependent scatter function). We are currently refining our microscopy techniques to obtain statistically representative images of the particle ensemble after the sample has been measured in the SAST. This will provide for detailed comparisons between the estimated particle geometries and the geometries observed in the SEM images.

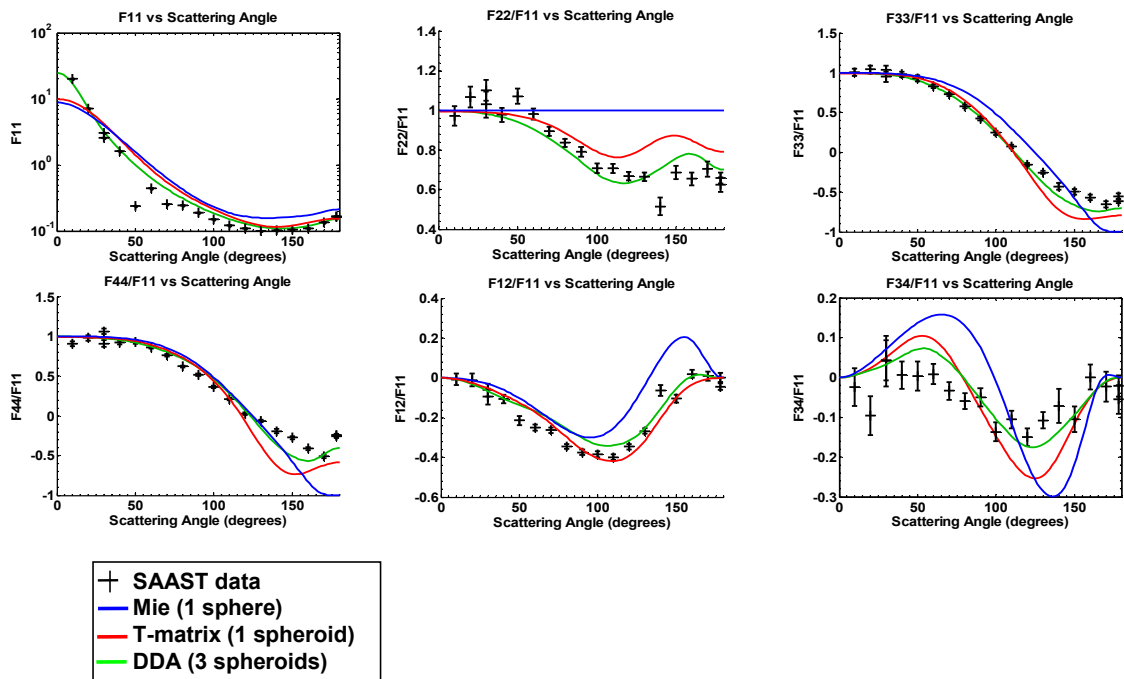


Figure 8: Scattering from a multi-spore Bg sample with comparison to Mie (spherical), T-Matrix (spheroidal) and multi-spore models. Note improvement in the element M_{22} fit due to the DDA model. Also, note that the measured element F_{11} has been renormalized such that the curves artificially overlie.

4. CONCLUSIONS

The SAST has been designed and constructed as a versatile optical signature testbed for aerosol characterization, demonstrating both aerosol ellipsometry and “lidar-in-a-box” capability. Only two example studies are presented in this report, whereas many studies have been performed on various samples at both NIR and MWIR wavelengths. Easily adaptable for other missions, the SAST is currently tasked with the measurement of infrared polarization phenomenology for biological agent detection. The polarization signature offers the possibility of discriminating certain bio-threats from backgrounds using IR radiation, avoiding most of the background radiation present in sunlight. The testbed is specially designed to measure both back- and oblique- angle polarization signatures, which are respectively applicable to Lidar signatures and useful for validating model predictions. Measurements from the SAST have compared well with model predictions. The SAST is continuously undergoing improvements, upgrades, and extensions and is currently being used for an extensive data collection campaign using a wide variety of biological simulants and interferents.

5. REFERENCES

- [1] Dougherty, G. M., Clague, D. S. and Miles, R. R., "Field-Capable Biodetection Devices for Homeland Security Missions," *Optics and Photonics in Global Homeland Security III* (Proc. SPIE 6540), 654016 (2007)
- [2] Shey, S. Y., Moshier, T. F. and Richardson, J. M., "Synergistic Standoff Sensor Concepts," in 7th Joint Conference on Standoff Detection for Chemical and Biological Defense Williamsburg, VA (2006)
- [3] Warren, J. W., Thomas, M. E., Rogala, E. W., Maret, A. R., Schumacher, C. A. and Diaz, A., "Systems engineering tradeoffs for a bio-aerosol lidar referee system," *Chemical and Biological Sensing V* (Proc. SPIE 5416), 204-215 (2004)
- [4] Buteau, S., Simard, J.-R., Déry, B., Roy, G., Lahaie, P., Mathieu, P., Ho, J. and McFee, J., "Bioaerosols laser-induced fluorescence provides specific robust signatures for standoff detection," *Chemical and Biological Sensors for Industrial and Environmental Monitoring II* (Proc. SPIE 6378), (2006)
- [5] Yee, E., Kosteniuk, P. R., Roy, G. and Evans, B. T. N., "Remote biodetection performance of a pulsed monostatic lidar system," *Applied Optics* 31(15), 2900-2913 (1992)
- [6] Marquardt, J. H., "Measurement of Bio-Aerosols with a Polarization-Sensitive, Coherent Doppler Lidar," in Fifth Joint Conference on Standoff Detection for Chemical and Biological Defense, Williamsburg, Virginia (2001)
- [7] Mayor, S. D., Spuler, S. M., Morley, B. M. and Loew, E., "Polarization lidar at 1.54 μm and observations of plumes from aerosol generators," *Optical Engineering* 46(9), 096201 (096211p) (2007)
- [8] Snow, J. W., Bicknell, W. E. and Burke, H.-h. K., "Polarimetric bio-aerosol detection: numerical simulation," *Chemical and Biological Standoff Detection III* (Proc. SPIE 5995), 59950Z (2005)
- [9] Pal, S. R. and Carswell, A. I., "Polarization Properties of Lidar Backscattering from Clouds," *Applied Optics* 12(7), (1973)
- [10] Snow, J. W., Bicknell, W. E., George, A. T. and Burke, H. K., "Standoff Polarimetric Aerosol Detection (SPADE) for Biodefense (TR-1100)," Lincoln Laboratory, Lexington, MA (2005)
- [11] Purcell, E. M. and Pennypacker, C. R., "Scattering and Absorption of Light by Nonspherical Dielectric Grains," *Astrophysical Journal* 185(705-714 (1973)
- [12] Richardson, J. M. and Aldridge, J. C., "The standoff aerosol active signature testbed (SAAST) at MIT Lincoln Laboratory," *Chemical and Biological Standoff Detection III* (Proc. SPIE 5995), 127-134 (2005)
- [13] Richardson, J. M., Aldridge, J. C. and Milstein, A. B., "Polarimetric lidar signatures for remote detection of biological warfare agents," *Polarization: Measurement, Analysis, and Remote Sensing VIII*, 69720E (2008)
- [14] Mishchenko, M. I. and Hovenier, J. W., "Depolarization of light backscattered by randomly oriented nonspherical particles," *Optics Letters* 20(12), 1356-1358 (1995)
- [15] Gimmetstad, G. G., "Reexamination of depolarization in lidar measurements," *Applied Optics* 47(21), 3795-3802 (2008)
- [16] Mullen, J., Bliss, N., Bond, R., Kepner, J., Kim, H. and Reuther, A., "High-productivity software development with pMatlab," *Computing in Science and Engineering* 11(1), 75-79 (2009)
- [17] Yurkin, M. A. and Hoekstra, A. G., "The discrete dipole approximation: An overview and recent developments," *Journal of Quantitative Spectroscopy and Radiative Transfer* 106(1-3), 558-589 (2007)